Electrical Conductivity and Ferromagnetism in a Reduced Graphene–Metal Oxide Hybrid

*Mohammad Razaul Karim, Hideaki Shinoda, Mina Nakai, Kazuto Hatakeyama, Hidenobu Kamihata, Takeshi Matsui, Takaaki Taniguchi, Michio Koinuma, Keita Kuroiwa, Mohamedally Kurmoo, Yasumichi Matsumoto, and Shinya Hayami**

The rare coexistence of ferromagnetism and electrical conductivity is observed in the reduced graphene oxide–metal oxide hybrids, rGO-Co, rGO-Ni, and rGO-Fe, using chemical reduction with hydrazine or ultraviolet photoirradiation of the graphene oxide–metal complexes, GO-Co, GO-Ni, and GO-Fe. The starting and final materials are characterized by X-ray photoelectron spectroscopy, transmission electron microscopy (TEM), elemental analysis, Mössbauer spectroscopy, and Raman spectroscopy. In contrast to graphene, where the electrical conductivity and magnetic properties are controlled by carrier (electron or hole) doping, those of graphene oxide can be controlled by complexation with Co^{2+}, Ni^{2+}, and Fe^{3+} cations through the strong electrostatic affinity of negatively charged graphene oxide towards metal cations. The presence of ferromagnetism and electrical conductivity in these hybrids can promote significant applications including magnetic switching and data storage.

1. Introduction

Magnetic property based on inorganic molecule and electronic conductivity originating from delocalized electron in organic materials can be unified through formation of organic-inorganic assembly, a common phenomenon for devising multifunctional hybrids with numerous fascinating applications.[1–4] These heterogeneous materials can be assembled by layering the organic and inorganic components alternately and the resultant hybrids exist like nano-composites with persistent individual properties.[3,4] Considering the self assembling tendency as the driving force it is possible to devise such hybrids showing ferromagnetism and metallic conductivity[5] or paramagnetism and superconductivity.[6] In addition, Coronado et al. have recently devised superconductive magnet using electrostatic interaction between self assembled distinct layers.[7]

Here, we consider unifying the conductivity of reduced graphene oxide (rGO) nanosheets and the magnetism of metal oxide (NiO, CoO, and Fe_2O_3) nanoparticles. Recently, physical or chemical modifications to graphene based materials have promised numerous potential applications such as electrocatalysis for oxidation of methanol (MeOH) and ethanol (EtOH); high performance electrochemical capacitors; stable, inert, and transparent fabricators for solar silicone cells; photocatalysts for hydrogen production from water; tunable electron transportable networks for photocurrent generation; and active materials for rechargeable batteries.[8–17] In most of the hybrids the dopant is trapped into the holey flat sheet of graphene through electrostatic attraction. As a result the structure and properties of graphene undergo modification and the selectivity and efficiency of the dopant materials are increased as well.[18–20] Though numerous research works have been carried out to control the light transparency, conductivity and electronic property, no significant work is noticed to study and modify the magnetism of graphene or graphene oxide (GO) hybrids though there exists recent evidence to manipulate graphene magnetism through formation of a graphene/Fe_3O_4 hybrid.[21] Due to the presence of various topological defects and coupling among the spin carriers, pure graphene has already been reported to show weak ferromagnetic long range ordering.[22,23]

M. R. Karim, H. Shinoda, M. Nakai, K. Hatakeyama, H. Kamihata, T. Matsui, Dr. T. Taniguchi, Dr. M. Koinuma, Prof. Y. Matsumoto, Prof. S. Hayami
Graduate School of Science and Technology
Kumamoto University
2-39-1 Kurokami, Chuo-ku, Kumamoto, 860-8555, Japan
E-mail: hayami@sci.kumamoto-u.ac.jp

M. R. Karim
Department of Chemistry
School of Physical Sciences
Shahjalal University of Science & Technology
Sylhet-3114, Bangladesh

Dr. T. Taniguchi, Dr. M. Koinuma,
Prof. Y. Matsumoto, Prof. S. Hayami
JST, CREST
5 Sanbancho, Chiyoda-ku, Tokyo, 102-0075, Japan

Dr. K. Kuroiwa
Department of Nanoscience
Faculty of Engineering
Sojo University
4-22-1, Ikeda, Nishi-ku, Kumamoto, 860-0082, Japan

Prof. M. Kurmoo
Laboratoire DECOMET
Institut de Chimie de Strasbourg
Université de Strasbourg
CNRS-UMR7177, 4 rue Blaise Pascal, Strasbourg 67000, France

DOI: 10.1002/adfm.201201418

Since the first experimental isolation, graphene has proved itself as an amazing material for its unique structural, mechanical and electronic properties.[24–26] Graphene nanosheets have one-atom thickness (≈3.4 Å) with planar sp^2 carbon atoms in symmetrical conjugated hexagonal cells, which are densely stacked to each other in a honeycomb crystal lattice of 1.42 Å bond length.[27] The remarkably high electrical conductivity of graphene arises from the flexible conductive layer of linearly combined π orbitals of sp^2 hybridized carbon atoms. To introduce ferromagnetism in graphene we consider doping magnetic nanoparticles in the 2D G matrix. But graphene itself being highly inert it is beyond the possibility to tie the positively charged metal ion or metal oxide through direct contact. On the other hand GO, the oxidized form of graphene can trap and locate the metal ions/nanoparticles successfully.[28,29] But the resultant hybrid we found is non-conductive as the sp^3 carbon sites bonded to extended carbonaceous functional groups of GO result in discontinuity of the conductive sp^2 network. However, the way to recover conductivity is the reduction of GO to rGO, by chemical agent or UV light irradiation according to recent report.[30]

Herein, we report the composite phenomenon including synthesis of non-conductive GO-metal ion complexes and their subsequent reduction to rGO-metal oxide hybrids showing both ferromagnetism and electrical conductivity.

2. Results and Discussion

2.1. Characterization and Bonding Mode of rGO-Metal Oxides

The single layer GO nanosheets were prepared and analyzed by atomic force microscopy (AFM) and X-ray photoelectron spectroscopy (XPS). GO-metal ion complexes (GO-Co, GO-Ni, and GO-Fe) were obtained by adding the metal ions to GO dispersion (**Figure 1**). The GO solution was brown in color and there was no precipitation. On the other hand, the brown precipitates for the GO-metal ion complexes appeared immediately after adding metal ions. When the GO-metal ion complexes were reduced by hydrazine or UV light irradiation, reduced rGO-metal oxide hybrids were obtained as black precipitates. The AFM image shows the single layer GO nanosheet (Figure S1, Supporting Information). The bonding mode of the metal oxide nanoparticles onto the rGO basal plane through electrostatic attraction was monitored by XPS, transmission electron microscopy (TEM), Raman spectroscopy, energy dispersive X-ray spectroscopy (EDS), Mössbauer spectroscopy, and magnetic analyses. XPS spectra for C1s of GO nanosheet, GO-metal ion complexes, and rGO-metal oxide hybrids (reduction by hydrazine or UV light irradiation) confirm the removal of oxygen from some of the oxygenated carbon sites of GO nanosheets. Pure GO nanosheets exhibit two individual peaks near 285 and 287 eV in their XPS spectra (Figure S2, Supporting Information). The peak for oxygenated C1s is more pronounced due to its narrower shape and higher height comparing with C1s peak for unoxidized carbon sites. But in practical calculation, the ratio of area under the peak for oxygenated C1s to the area under the peak for all C1s carbon sites (oxygenated and unoxygenated) is found to be 50% (3.9, 32.3, 6.3, and 7.5 for C—O, C—O—C, C=O, and O=C—O functional sites, respectively, calculated through advantage spectrum processing software). This value corresponds to 30% atomic ratio of O to total amount of C and O. Recently, we observed that the ratio of oxygenated C1s peak area to total C1s peak area in XPS spectra is proportional to the extent of oxidation which is expressed in terms of atomic ratio of O to total amount of carbon and oxygen atom present in the GO sample. Pure GO dispersions synthesized in different batches were used for GO-Co, GO-Ni and GO-Fe complexes. The merging of oxygenated C1s peak and unoxygenated C1s peak is more for GO-Fe which indicates higher extent of graphite oxidation during synthesis of this GO sample. Covalently bonded carbon atoms have no affinity for incoming metal ions, as a result the peaks around 285 eV (**Figure 2**), which remain unchanged during the reduction is concluded to arise from C—C, C=C, and C—H bonds for all the samples. This observation matches with some previously reported result.[30] Oxygen containing carbonaceous groups of GO exist in the form of epoxide (—O—), hydroxyl (—OH) groups located in the basal plane with XPS peak position at 286.8–287.0 eV and carbonyl (—C=O), carboxyl (—COOH) at the edge with peak position at 287.8–288.0 eV and 289.0–289.3 eV, respectively.[31–33] During reduction the decrease in peak height near 287 eV indicates destruction of some epoxy and hydroxyl group. However, at the end of reduction these peaks are not completely disappeared which indicates that some epoxy and hydroxyl groups are unaffected towards reduction.

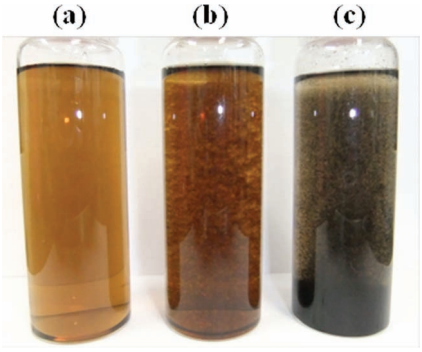

Figure 1. Photographs of the sample: a) GO nanosheets dispersed in water solution, b) the precipitation of GO-metal complexes, and c) the precipitation of rGO-metal oxide hybrids.

Another evidence for the unchanged part of epoxy sites is the lower conductivity of the rGO hybrids than graphene. As the difference between the conductivity of GO and graphene rises due to the breakthrough of conductive sp^2 network in graphene by replacement of some sp^3 carbon sites having epoxy groups, our measured lower conductivity of rGO than pure graphene suggests the presence of some epoxy groups remaining still after reduction. We propose the attachment of metal ions to some partially negative epoxy or hydroxyl oxygen through coulombic force prohibit further reduction of this oxygenated sites by repulsing hydrazine molecules from this metal masked oxygen, a phenomenon reverse to the mechanism reported for hydrazine reduction of GO.[34]

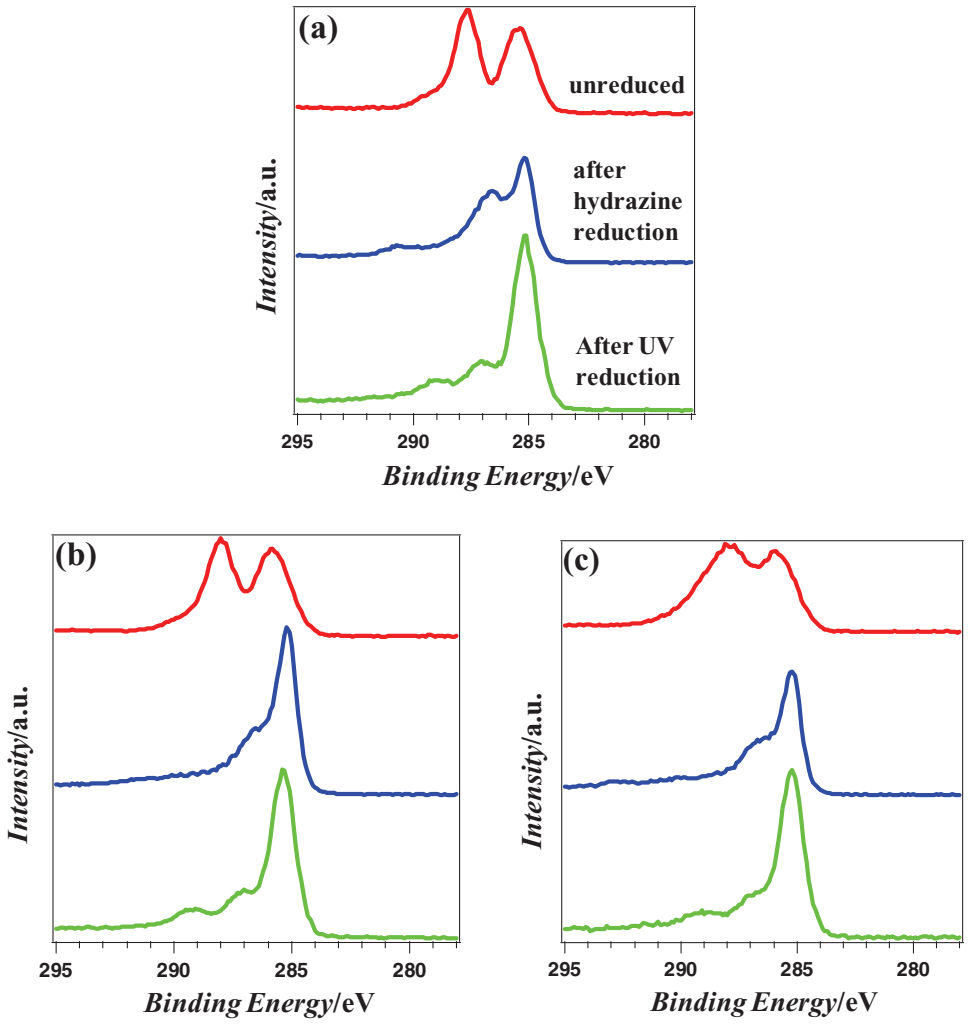

Figure 2. XPS spectra of C1s of a) GO-Co, b) GO-Ni, and c) GO-Fe complexes. Unreduced, hydrazine-reduced, and UV-irradiation-reduced samples are shown with red, blue, and green lines, respectively.

When rGO is converted to rGO-metal oxide hybrids, the electron cloud on oxygen atom and the π orbital of C=O bonds become more localized and interact with metals d-π orbital, which could be responsible for the merging of two peaks almost into one. In case of metal precursor, peak height for 2p electrons of starting metal ions Co^{2+}, Ni^{2+} and Fe^{3+} remain unchanged during reduction, which suggests that the metal ions do not undergo reduction by the reducing agent, though there was some possibility (Figure S3, Supporting Information). Besides the binding energy for $2p_{3/2}$ peak of Co is shifted by 0.5 eV (from 781.8 to 781.3 eV) for conversion of Co^{2+} ion into CoO nanocomposite in rGO-Co hybrid. The electron density around the Co nucleus is increased due to the attachment of electron rich oxide ion. The binding energy is inversely proportional to electron density, so the higher the electronic density the lower is the binding energy. The figures therefore implies the formation of CoO during reduction of the hybrids. Similar observation is noticed for all the samples. In addition, the Mössbauer spectrum confirms the +3 oxidation state of the attached Fe ion. The formation of metal oxide nanocluster is indicated by magnetic study where the Néel temperature resemblance to nanoparticles of corresponding oxides. Based on these observations we suggest existence of electrostatic bonding between metal oxide nanoparticles and rGO nanosheets for all the hybrids (**Scheme 1**). Firstly, some primary metal ions bound to some of the partially charged oxygenated sites of GO nanosheets and prohibit these sites being reduced by hydrazine molecules. These grow gradually by attracting oxygen atoms, metal oxide molecules (produced during reduction process) and more free metal ions. Finally irregular shaped metal oxide nanoparticles become anchored to the rGO matrices by Columbic force.

The question also arises about identification of the most important functional sites for attachment of the metal ions. Mikhoyan et al. have elucidated the atomic and electronic structure of GO and reported that 85% of oxygenated carbon atoms are sp^3 hybridized and associated to epoxy groups (—O—C) whereas, the remaining 15% belongs to hydroxyl or carboxyl groups (C—OH, COOH).[29] From statistical consideration, mostly available epoxy sites are the best for attaching metal ions. Besides, the epoxy groups locate interior of the GO islands, but

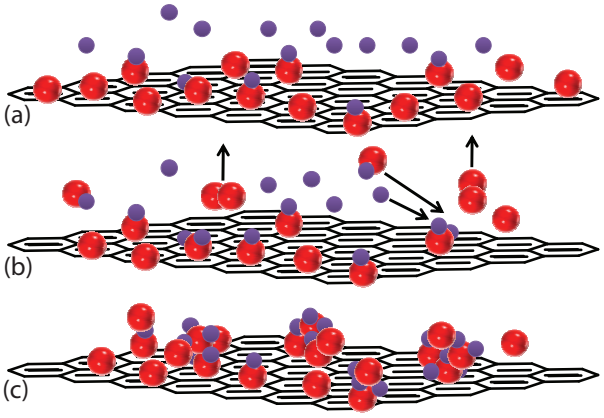

Scheme 1. Formation of rGO–metal oxide nanoparticle hybrids. a) Negatively charged oxygenated site (red) of GO attract some primary metal ions (violet) through columbic force. b) During reduction some oxygen escapes from the system, whereas metal masked oxygenated sites remain unreduced and attract metal oxide, oxygen, and additional metal ions. c) Finally, gradual deposition results in irregularly shaped metal oxide nanoparticles anchored on rGO matrices.

vast majority of hydroxyl carbon sites locate at the circumference. Practically in TEM images the locations of nanoclusters interior of GO fragment indicate their association with epoxy functional sites. Also from theoretical consideration, it is not surprising that every epoxy oxygen associated to two sp^3 carbon is more polar than a hydroxyl oxygen attached to a single sp^2 carbon atom towards coulombic interaction with the metal ions. The electrostatic repulsion of charged GO nanosheet, which is common for charged colloidal dispersion, is the cause behind the exfoliation of massive graphite oxide into GO dispersion. Addition of positively charged transition metal ions into GO dispersion neutralizes the negative charge of GO through formation of GO-M complex accompanying coagulation of exfoliated layers as observable solid mass. Many hybrids have been reported up to date but no feasible way has been found out to identify the quantitative ratio of functional groups attacking the incoming ions. Our future attention is based on solid-state NMR analysis to solve this puzzle. We suppose that ^{13}C NMR in combination with XPS spectra of the hybrid samples with varied metal ion concentration could be employed to depict the exact quantitative picture of functional carbon sites likely to attract the metal ions with highest priority. Nevertheless, the hybrids having magnetic metal ions would not facilitate NMR analysis. The possible alternative we can consider is to leach out metal oxide nanoparticles through isotopically labeled acid (DCl) treatment followed by tracer analysis to locate the labeled deuterium atom responsible for replacement of metal ions.

Figure 3 illustrates the TEM images of rGO-metal oxide hybrids. Random location of metal oxide nanoparticles on rGO is observed. The images imply that only rGO-Ni exists in single layer whereas, in rGO-Co and rGO-Fe, coagulation indicates folding of graphene sheets. Also in case of rGO-Ni no blackish dense spot is noticed, which implies the possibility of hydroxide formation. Hydroxide exists in layers and unlike metal oxide nanoparticles they cannot be identified usually through dense spot. Alternatively, there could be a sandwich like decorating where nickel ions locate within the rGO layers. rGO sheets trap the metal ions first by electrostatic attraction and anchor the metal oxides finally in the 2D holey carbon matrix. In Figure 3c the accommodation of Fe atom is more pronounced comparing with those of Co (Figure 3a) and Ni (Figure 3b) atoms. Statistical analysis revels that the black dense spots cover ≈80% of the surface. This observation can be explained it terms of electropositivity and ionic size. The trend in electropositivity and atomic radii of these three ions are $Fe^{3+} > Co^{2+} > Ni^{2+}$ and $Co^{2+} > Ni^{2+} > Fe^{3+}$. Apparently, high charge and smaller size facilitate iron mostly over cobalt and nickel to migrate and localize itself inside the negative GO sheet. The extent of interactions between rGO and metal oxide nanoparticles is further governed by the exchangeability of oxygen atom from carbon edge of graphene layer to the metal ion. Fe^{3+} ion having itself more affinity toward oxygen easily dispersed in rGO. EDS confirm incorporation of metal centers inside the rGO nanosheet. The elemental analyses show presence of corresponding metal oxides in each sample (Figure S4, Supporting Information), and the peak for Cu is noticed as the sampling was performed on Cu grids.

Raman spectroscopy is among the most useful kit to study change and doping on GO. Both the hole and electron doping result in shifting the G-band in Raman spectrum and the intensity ratio of D and G-band varies sensitively with doping.[35] Raman spectra of rGO-Co hybrid show two bands at 1580 cm^{-1} (G band), and 1350 cm^{-1} (D band) which confirm the presence of carbon materials (**Figure 4**). Similar observations were found for Ni and Fe hybrids. The G and D bands are responsible for E_{2g} photon corresponding to sp^2 atoms and κ-point photon of A_{1g} symmetry of breathing mode resulting from local defects and disorder.[36,37] Peak ratio (I_D/I_G) gradually decreases along the conversion: GO → GO-metal ion hybrids → rGO-metal oxide hybrids. The I_D/I_G is inversely proportional to the extent of sp^2 domain.[38] Therefore, gradual decrease in this value implies diffusion of this domain which agrees with the observation from XPS study.

Though XPS analysis and EDS spectra confirmed about the oxidation state of metal ion in the hybrids, we further justified the ionic nature by Mössbauer spectroscopy for the rGO-Fe hybrid at room temperature (**Figure 5**). A doublet with quadruple splitting (Q.S.) = 0.760 mm s^{-1} and isomer shift (I.S.) = 0.349 mm s^{-1} was observed for rGO-Fe hybrid at 300 K. This

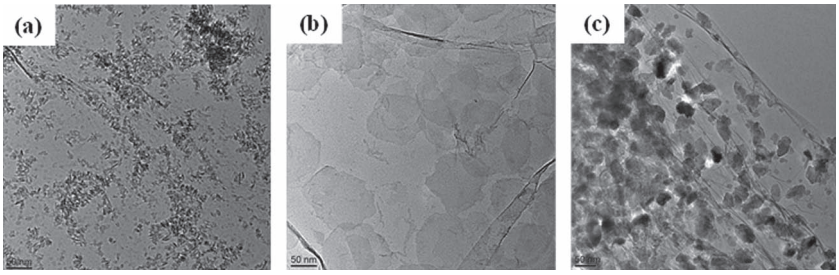

Figure 3. TEM images of rGO-metal oxide hybrids: a) rGO-Co, b) rGO-Ni, and c) rGO-Fe.

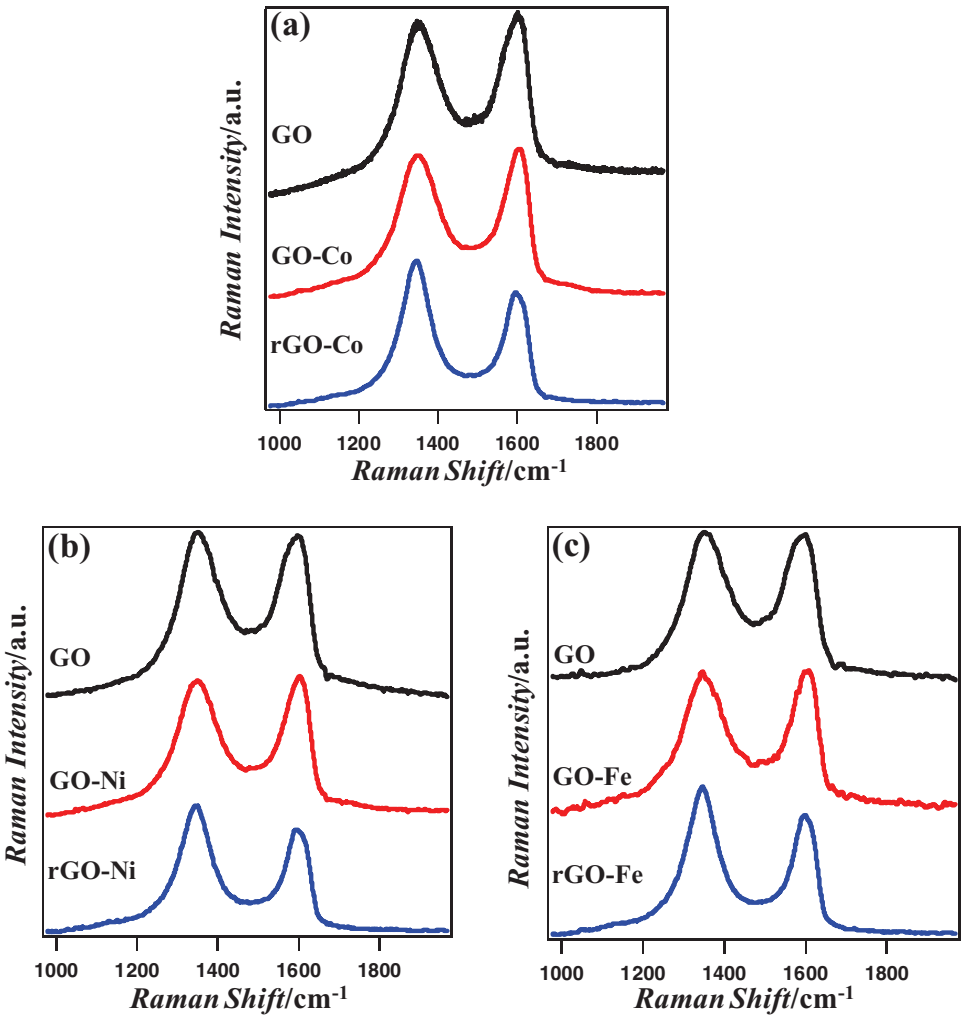

Figure 4. Raman spectra of a) GO-Co, b) GO-Ni, and c) GO-Fe complexes. GO (black), GO-metal complex (red), and rGO-metal hybrid (blue).

result confirms presence of Fe^{3+} ion in the rGO-Fe hybrid. In case of Ni and Co hybrid, we consider similar model from this study.

2.2. Conductive Nature of the Hybrids

Pure GO is an insulator.[19] The conductive nature of all hybrids was measured along the surface of aggregated nanosheets during the course of photoreduction period. Conductivity measurement with respect to hydrazine reduction time was not possible since, the reduced sample converted to coagulated solid mass. (**Figure 6**) shows the *I–V* curves with respect to photoreduction time measured by AFM. The current is passed across the single layer hybrid sheet and thus express the conductivity across the GO/rGO basal plane. At the initial time, unreduced GO-metal complexes show almost zero conductivity irrespective of the magnitude of applied voltage. The current increases with voltage almost linearly with irradiation time. Extent of reduction is proportional to duration of irradiation so it implies that only the reduced form carries current. After 24 h of photoirradiation all the hybrids exhibited maximum conductivity. The current conductivity is near 40, 20, and 10 μA for rGO-Co, rGO-Ni, and rGO-Fe hybrids, respectively. The conductivity remains after switching off the light source.

2.3. Ferromagnetic Nature of the Hybrids

We used both the UV and hydrazine reduced samples for magnetic study whereas, significant responses were found in cases of hydrazine-reduced samples. UV is a weak reducing agent and can reduce the GO sheets superficially, but for magnetic measurement the bulk sample responds properly. **Figure 7** represents the magnetization as a function of temperature. The magnetic behavior of pure graphene has been found to display both ferromagnetism and antiferromagnetism.[23] In contrast, the rGO-metal oxide hybrids display a long-range magnetic ordering in case of rGO-Co and rGO-Ni where the field cooled magnetization (FCM)-zero field cooled magnetization (ZFCM)

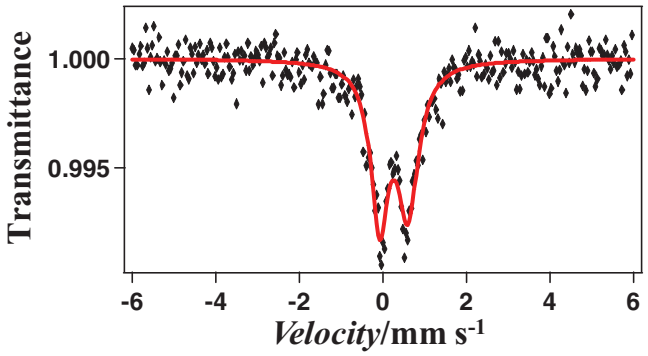

Figure 5. Mössbauer spectrum of rGO-Fe hybrid after reduction with hydrazine at room temperature.

bifurcates at 11 and 15 K, respectively. In case of rGO-Fe, the bifurcation is sluggish and observed at ca. 30 K. In absence of the structural features of metal-oxides or metals we are left with only hypotheses to explain the observed behaviors. Although the three elements (Fe, Co, and Ni) are ferromagnets, their critical temperatures are very high and if they exist as nanoparticles then a blocking temperature corresponding to the observed ones may be possible.[39–41] However, we can rule out the presence of metallic nanoparticles on chemical ground since it is not likely that these high-valent metals be reduced to the elements by UV-irradiation. Furthermore, the sharp bifurcation in case of rGO-Co and rGO-Ni are atypical for the behaviors of metallic nanoparticles, which are broader. Furthermore, the reproducibility of the data for different batches is not in agreement to the expected behavior of metallic nanoparticles. Also the possibility for formation of metallic nanoparticles is disfavored by the low value for Néel temperature. In a previous study Zhang et al. reported the Néel temperature for Co nanoparticles as 150 K as well for bulk CoO this value is 293 K, which are much higher than our current observation.[42] However, for rGO-Fe the FCM-ZFCM curves may originate from nanoparticles. The second hypothesis is that the metal ions are in the form of oxides on the graphene sheets. Given that NiO, CoO are antiferromagnets we can eliminate the possibility of these species. By the same argument Co_2O_3 or Co_3O_4 can be eliminated (also XPS analysis reveals that there is no evidence for the formation of Co_2O_3 or Co_3O_4). However, iron oxides are either ferrimagnet or canted antiferromagnets depending on the phase and thus can be responsible for the observed results. The next candidate in our hypotheses could be the presence of the hydroxides of

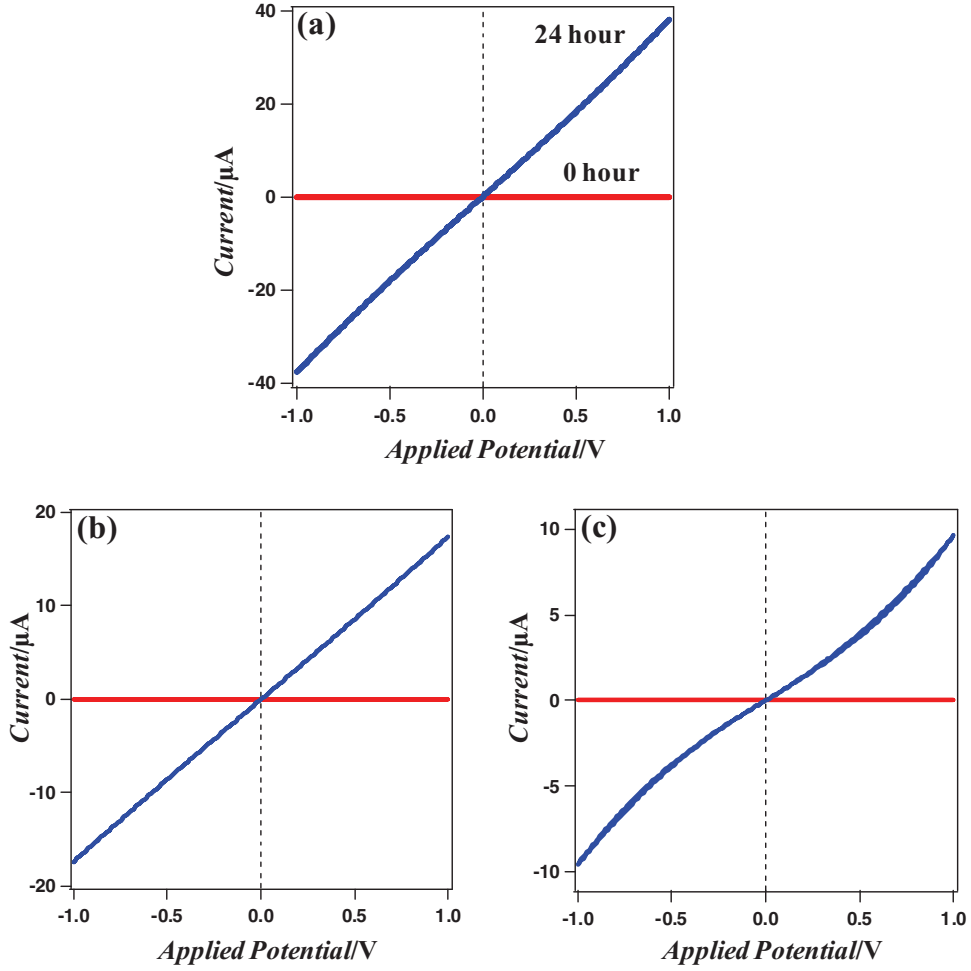

Figure 6. Current vs. applied voltage for a) GO-Co, b) Go-Ni, and c) GO-Fe nanosheets before and after photoreduction.

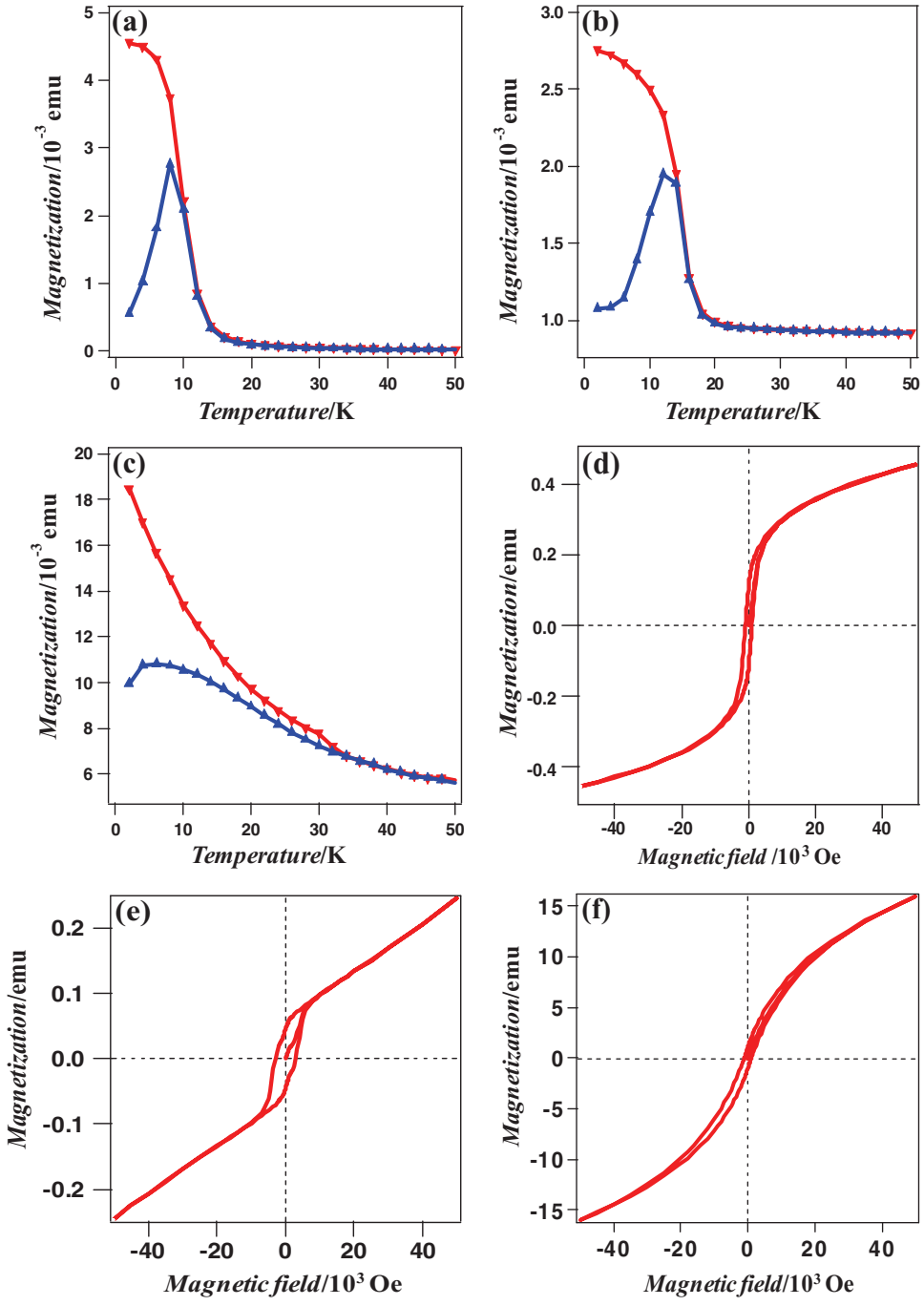

Figure 7. Magnetic properties of the hybrids. Temperature dependence of FCM (red) and ZFCM (blue) measured at 5 Oe are as a) rGO-Co, b) rGO-Ni, and c) rGO-Fe. Field dependence of the magnetizations at 2 K. Magnetic hysteresis loops observed for e) rGO-Co, f) rGO-Ni, and g) rGO-Fe.

Co and Ni which are layered and can match the graphene structure as well as they consist of ferromagnetic layers. Thus, they can be expected to behave as the observed results, if the layers are single. However, they are antiferromagnetically couple to neighboring layers in the bulk to give fully compensated antiferromagnets. The last possible scenario is that the moments of the metal ions are coupled by Ruderman-Kittel-Kasuya-Yoshida (RKKY) exchange through the conduction electrons of the graphene moiety to result in long-range magnetic ordering even if the metal moments are far apart and randomly located on the graphene surface. Of all the hypotheses, the last two are the most probable ones and it would require further experimentation beyond our present capacity.

Magnetic properties of nanoparticles are strongly dependent on size, shape and imperfections.[43,44] Size dependability can be explained by two previously established phenomena. Firstly,

nanoparticles can undergo coalescence to form 2D planer structure similar to a sheet when the particle sizes are very small. In such case the magnetic anisotropy was reported to originate from electronic delocalization and symmetry breaking.[45] Also the extent of magnetization and effect on magnetic anisotropy of thin film of this type was found to depend on the substrate where it grows.[46,47] Secondly, in case of larger sized particles aggregation results dispersed 3D mass where the magnetization value depend on the surface to volume ratio as it is well known that particles such as Co, Fe and Ni staying in the surface of a 3D nanoclusters generate magnetic anisotropy perpendicular to the surface plane. Unlike planer sheet, in case of dispersed 3D masses the role of substrate on magnetizainon is still unclear. In case of our synthesized hybrids the TEM image clearly indicates the dispersion of distinct nanoclusters, which resemble with the second type of above and thus we can omit the possibility of any type of magnetic coupling between the trapped particles and sub lattice rGO matrices except the hypothesis of RKKY exchange.

Beside this theoretical consideration, still question rises about existence of ferromagnetism in rGO itself. The present rGO nanosheets have many holes and therefore many edges. To evaluate the states of defect arising from carbons in holes and edges of rGO nanosheets, we measured the magnetic properties of rGO nanosheets after running the photoreduction for 48 h (Figure S5, Supporting Information).[48] FCM and ZFCM curves obtained at 100 Oe start to diverge at about 300 K, whereas no divergence was observed for the GO virgin sample (nearly zero magnetization). The contamination of metals such as 3d transition metals in the rGO was below the limit of detection (<0.001% in ICP-AES). Furthermore, the present rGO nanosheets exhibited magnetic hysteresis at 2 and 300 K (Figure S5b, Supporting Information). No hysteresis was observed for the hydrazine-reduced rGO samples. Consequently, the ferromagnetic behavior is attributable to the photoreduction, not contamination. For a 1.0 mg rGO sample containing 0.001% Fe metal (saturation magnetization, 220 emu g^{-1}) as an impurity, the magnetization would be about 2.2×10^{-6} emu in the present test, which is much smaller than the results shown in Figure S5 (Supporting Information; $>5 \times 10^{-5}$ emu). Graphene generally has zigzag and armchair edges. Armchair edges have no localized spin because they consist of only π and π^* bands. On the other hand, the zigzag edges have localized spins because they have an antibonding flat band with π and π^* bands. Thus, the ferromagnetic behavior of the rGO nanosheets (there is a similar report for other rGO prepared by thermal annealing with hydrazine treatment) produced by the photoreaction indicates that there are zigzag edges and/or CH bonds in holes and/or edges. Therefore, ferromagnetic property of the rGO used in the present case is very weak, and almost is diamagnetism. Beside our observation, unlike graphene no reported evidence exist for ferromagnetic nature of GO. In case of GO the oxygenated functional groups are extended perpendicularly outward from opposite sides of 2D GO plane. This structure is much distinct than graphene symmetry and might alter the magnetic anisotropy. However, the real intrinsic phenomenon behind the loss of ferromagnetism for modification of G to GO is still unknown. Microporous matrix can increase the interparticle magnetic and electronic coupling among the guest nanoclusters and host matrix. Same way the role of microporous rGO matrices is to intensify the coercive harmony among the dispersed nanoclusters, which we suggest similar to the phenomenon reported by Tolbert et al. for cobalt nanoparticles confined at silica cells having hexagonal honeycomb structure like graphene.[49]

The shapes of the hysteresis loops in the isothermal magnetization at 2 K of rGO-Co and rGO-Ni are more typical of those of molecular magnets rather than those of nanoparticles of metals or oxides. Thus the observed data are more inclined to favor the presence of a molecular system rather than metallic particles, again leading to the last two hypotheses brought forward above. The rGO is a well-known conductor for micro-electronics. The present work brings in addition enhanced ferromagnetism to this conductor. This dual property is important for micro-level step-up or step-down transformation of electricity. Our future aspect is to fit these new hybrids for core materials in micro-level energy tuning devices.

3. Conclusions

We have synthesized ferromagnetic rGO-metal oxide hybrids with conductivity. Graphene-based materials with these dual functional properties are reported here for the first time. The synthetic route is reproducible, simple, and affordable under mild conditions. Firstly, negative GO nanosheets show strong electrostatic attraction toward positively charged metal ions to form GO–metal complexes. These complexes undergo reduction accompanied by a shift of some oxygen atoms from the GO precursor to metal ions and the rGO–metal oxide hybrid is formed finally. The chemical change in the GO moiety during reduction was confirmed by XPS, TEM, and Raman studies. EDS, XPS, and Mössbauer spectra confirm the existence of the metal ion in the rGO-metal oxide hybrids. The magnetic data indicate the formation of metal oxide nanoparticles anchored to the rGO matrices. GO-metal ion complexes are insulators, but the chemically or photoreduced rGO-metal oxide hybrids are conductors. The destruction of epoxy groups bonded to graphene precursor is responsible for increasing the conductivity. During the course of photoirradiation, large non-conductive aromatic moieties within the GO nanosheets split into numerous sp^2 conductive fragments that assemble in a two electrode system resulting increased conductivity. All the rGO-metal oxide hybrids are ferromagnetic with significant deviation in magnetic properties from original graphene. The anchored metal oxide nanoparticles on the rGO nanosheets are responsible for the ferromagnetism. Due to the modified magnetic and conductive nature, we expect future applications of theses hybrids in electrochemical capacitors, energy tuning devices for microelectronics, and cheaper materials for data storage and magnetic switching.

4. Experimental Section

GO was synthesized by slight modification to Hummer's method.[50] Graphite powder (1 g, 300 μm, Wako Ltd), $NaNO_3$ (1.0 g, fine mesh) and H_2SO_4 (48 mL, 97%) was cooled by stirring in an ice bath for 15 min.

$KMnO_4$ (3.0 g, fine mesh) was added slowly with vigorous stirring maintaining the temperature below 20 °C. After 20 min the mixture was warmed and maintained at 35 ± 3 °C for 30 min. Then 180 mL water was added slowly, the temperature rose gradually and was kept in 95 ± 3 °C for another 30 min. It was further diluted by adding 400 mL water. Finally H_2O_2 (30%, 12 mL) was added to convert the unreacted permanganate and manganese dioxide into soluble salts. The mixture was centrifuged (3000 rpm, 10 min.) and the precipitate was washed with 5% HCl solution (1 time) and water (3 times). The final precipitate was dried at 70 °C for 24 h. It was then dispersed in water (1 mg/5 mL) by 2 h of sonication, followed by discarding aggregated carbon through centrifugation at 4000 rpm for 1 h.

GO-metal ion complexes were directly precipitated from a mixture of GO dispersion (20 mL) and metal chloride hydrate ($CoCl_2{\cdot}6H_2O$, $NiCl_2{\cdot}6H_2O$, $FeCl_3{\cdot}6H_2O$,) solution (5 mg salt in 20 mL water) at 25 °C for 12 h. The metal chloride changed from brown colors solution to dark dispersion. The pH of the solutions turned to more basic at the end of reaction. For chemical reduction, GO-metal ion complex dispersion (10 mL) was refluxed with hydrazine (0.64g, 20 mmol) at 100 °C for 24 h. Black residue finally appeared. For photoreduction, the samples were directly exposed to 365 nm light beam from an ultrahigh pressure mercury lamp (500 W; Optical Modulex, 5X-UI500HQ, Usino) for 24 h.

AFM (Digital Instruments, Nanoscope V, tapping mode) was employed to study surface morphology. The mica substrate was preferred as atomic level smooth surface was possible to reproduce by erasing the surface several times with gummed polymer tape. Additionally polar mica surfaces have strong affinity toward the samples to produce persistent layer. Droplets of dilute sample solution were spread on surface of 1 cm^2 mica substrate followed by drying under high vacuum. Gradual dilutions of the samples were continued until having single layer GO nanosheet.

XPS (Thermo Scientific, Sigma Probe) was used to analyze the surface of GO nanosheets. A monochromatized X-ray source (Al Kα, $h\nu$ = 1486.6 eV) was used for XPS, and a discharge source (He I, $h\nu$ = 21.2 eV) was used for ultraviolet photoelectron spectroscopy (UPS) in the same instrument for XPS. In this measurement, a Pt substrate (GO/Pt film) was used to determine the Fermi level. All measurements were done in a vacuum better than 10^{-7} Pa. Emitted electrons were detected by a hemispherical energy analyzer equipped with six channeltrons.

A micro Raman spectrometer (NRS-3100, Jasco, Japan) with a 532 nm excitation source at room temperature was used to collect the Raman spectra.

To perform elemental analyses by energy dispersive X-ray spectroscopy (EDS) and TEM (FEI Company, TECNAI-20, 200 kV), one drop of the aqueous nanosheet suspension was deposited on a holey carbon film.

The conductivities along the surface of GO-metal ion complexes and r-GO-metal oxide hybrids were measured by a two electrode system. The working electrode was composed of two 90 mm thick comb Au electrodes (60 bars each, 2 μm distance) assembled face to face on a glass substrate. GO-metal ion complexes dispersion was poured dropwise to soak the electrodes and then it was allowed to dry. The conductivity of this assembly was monitored with respect to photo-irradiation time.

The Mössbauer spectrometer with a Co/Rh source was driven in the transition mode. The measurements at low temperature were performed with a closed-cycle helium refrigeration (Iwatani Co. Ltd).

A Quantum Design MPMSXL-5 superconducting quantum interference device (SQUID) magnetometer was used for magnetization measurements. The samples were placed inside the SQUID chamber, and the field dependence of the magnetization was measured at 2 K.

Supporting Information

Supporting Information is available from the Wiley Online Library or from the author.

Acknowledgements

This work was supported by Innovative Areas "Coordination Programming" (area 2107) from the MEXT, Japan.

Received: May 26, 2012
Revised: July 13, 2012
Published online: August 27, 2012

[1] A. K. Cheetham, C. N. R. Rao, *Science* **2007**, *318*, 58.
[2] F. Hoffmann, M. Cornelius, J. Morell, M. Fröba, *Angew. Chem. Int. Ed.* **2006**, *45*, 3216.
[3] C. Sanchez, B. Julian, P. Belleville, M. Popall, *J. Mater. Chem.* **2005**, *15*, 3559.
[4] C. Sanchez, B. Lebeau, F. Chaput, J. P. Boilot, *Adv. Mater* **2003**, *15*, 1969.
[5] E. Coronado, J. R. Galán-Mascarós, C. J. Gómez-García, V. Laukhin, *Nature* **2000**, *408*, 447.
[6] E. Ojima, H. Fujiwara, K. Kato, H. Kobayashi, *J. Am. Chem. Soc.* **1999**, *121*, 5581.
[7] E. Coronado, C. Marti-Gastaldo, E. Navarro-Moratalla, A. Ribera, S. J. Blundell, P. J. Baker, *Nat. Chem.* **2010**, *2*, 1031.
[8] E. J. Yoo, T. Okata, T. Akita, M. Kohyama, J. Nakamura, I. Honma, *Nano Lett.* **2009**, *9*, 2255.
[9] L. Dong, R. R. S. Gari, Z. Li, M. M. Craig, S. Hou, *Carbon* **2010**, *48*, 781.
[10] Z. S. Wu, D. W. Wang, W. Ren, J. Zhao, G. Zhou, F. Li, H. M. Cheng, *Adv. Funct. Mater.* **2010**, *20*, 3595.
[11] H. Yu, S. Chen, X. Fan, X. Quan, H. Zhao, X. Li, Y. A. Zhang, *Angew. Chem. Int. Ed.* **2010**, *49*, 5106.
[12] L. Jia, D. H. Wang, Y. X. Huang, A. W. Xu, H. Q. Yu, *J. Phys. Chem. C* **2011**, *115*, 11466.
[13] H. Hayashi, I. V. Lightcap, M. Tsujimoto, M. Takano, T. Umeyama, P. V. Kamat, H. Imahori, *J. Am. Chem. Soc.* **2011**, *133*, 7684.
[14] C. Xu, X. Wang, J. W. Zhu, *J. Phys. Chem. C* **2008**, *112*, 19841.
[15] D. H. Wang, D. W. Choi, J. Li, Z. G. Yang, Z. M. Nie, R. Kou, D. H. Hu, C. M. Wang, L. V. Saraf, J. G. Zhang, I. A. Aksay, J. Liu, *ACS Nano* **2009**, *3*, 907.
[16] S. M. Paek, E. Yoo, I. Honma, *Nano Lett.* **2009**, *9*, 72.
[17] G. Goncalves, P. Marques, C. M. Granadeiro, H. I. S. Nogueira, M. K. Singh, J. Gracio, *Chem. Mater.* **2009**, *21*, 4796.
[18] N. Yang, J. Zhai, D. Wang, Y. Chen, L. Jiang, *ACS Nano* **2010**, *4*, 887.
[19] B. Seger, P. V. Kamat, *J. Phys. Chem. C* **2009**, *113*, 7990.
[20] G. Williams, P. V. Kamat, *Langmuir* **2009**, *25*, 13869.
[21] J. Liang, Y. Xu, D. Sui, L. Zhang, Y. Huang, Y. Ma, F. Li, Y. Chen, *J. Phys. Chem. C* **2010**, *114*, 17465.
[22] Y. Wang, Y. Huang, Y. Song, X. Zhang, Y. Ma, J. Liang, Y. Chen, *Nano Lett.* **2009**, *9*, 220.
[23] M. H. S. S. Ramakrishna, K. S. Subrahmanyam, C. N. R. Rao, *J. Phys. Chem. C* **2009**, *113*, 9982–9985.
[24] K. S. Novoselov, A. K. Geim, S. V. Morozov, D. Jiang, Y. Zhang, S. V. Dubonos, I. V. Grigorieva, A. A. Firsov, *Science* **2004**, *306*, 666.
[25] R. F. Service, *Science* **2009**, *324*, 875.
[26] A. K. Geim, *Science* **2009**, *19*, 1530.
[27] A. K. Geim, K.S. Novoselov, *Nat. Mater.* **2007**, *6*, 183.
[28] W. W. Cai, R. D. Piner, F. J. Stadermann, S. Park, M. A. Shaibat, Y. Ishii, D. X. Yang, A. Velamakanni, S. J. An, M. Stoller, J. H. An, D. M. Chen, R. S. Ruoff, *Science* **2008**, *321*, 1815.
[29] K. A. Mikhoyan, A. W. Contryman, J. Silcox, D. A. Stewart, G. Eda, C. Mattevi, S. Miller, M. Chhowalla, *Nano Lett.* **2009**, *9*, 1058.
[30] Y. Matsumoto, M. Koinuma, S. Y. Kim, Y. Watanabe, T. Taniguchi, K. Hatakeyama, H. Tateishi, S. Ida, *Appl. Mater. Int.* **2010**, *2*, 3461.

[31] T. Szabó, O. Berkesi, P. Forgó, K. Josepovits, Y. Sanakis, D. Petridis, I. Dékány, *Chem. Mater.* **2006**, *18*, 2740.
[32] D. W. Boukhvalov, M. I. Katsnelson, *J. Am. Chem. Soc.* **2008**, *130*, 10697.
[33] Z. Li, W. Zhang, Y. Luo, J. Yang, J. G. Hou, *J. Am. Chem. Soc.* **2009**, *131*, 6320.
[34] X. Gao, J. Jang, S. Nagase, *J. Phys. Chem. C* **2010**, *114*, 832.
[35] A. Das, S. Pisana, B. Chakraborty, S. Piscanec, S. K. Saha, U. V. Waghmare, K. S. Novoselov, H. R. Krishnamurthy, A. K. Geim, A. C. Ferrari, A. K. Sood, *Nat. Nanotechnol.* **2008**, *3*, 210.
[36] F. Tuinstra, J. L. Koenig, *J. Chem. Phys.* **1970**, *53*, 1126.
[37] A. C. Ferrari, J. Robertson, *Phys. Rev. B* **2000**, *61*, 14095.
[38] L. G. Cançado, K. Takai, T. Enoki, M. Endo, Y. A. Kim, H. Mizusaki, A. Jorio, L. N. Coelho, R. Magalhães-Paniago, M. A. Pimenta, *Appl. Phys. Lett.* **2006**, *88*, 163106.
[39] J. T. Richardson, L. W. Veron, *J. Phys. Chem.* **1958**, *62*, 1153.
[40] G. Wang, X. Shen, J. Horvat, B. Wang, H. Liu, D. Wexler, J. Yao, *J. Phys. Chem. C* **2009**, *113*, 4357.
[41] Y. Ichiyanagi, N. Wakabayashi, J. Yamazaki, S. Yamada, Y. Kimishima, E. Komatsu, H. Tajima, *Physica B* **2003**, *329*, 862.
[42] G. H. Wena, R. K. Zheng, K. K. Fung, X. X. Zhang, *J. Magn. Magn. Mater.* **2004** *270*, 407.
[43] M. R. Diehl, J. Y. Yu, J. R. Heath, G. A. Held, H. Doyle, S. Sun, C. B. Murray, *J. Phys. Chem. B* **2001**, *105*, 7913.
[44] D. L. Leslie-Pelecky, R. D. Rieke, *Chem. Mater.* **1996**, *8*, 1770.
[45] C. Chappert, K. L. Dang, P. Beauvillain, H. Hurdequint, D. Renard, *Phys. Rev.B* **1986**, *34*, 3192.
[46] F. J. A. den Broeder, W. Hoving, P. H. J. Bloemen, *J. Magn. Magn. Mater.* **1991**, *93*, 562.
[47] F. Wilhelm, U. Bovensiepen, A. Scherz, P. Poulopoulos, A. Ney, H. Wende, G. Ceballos, K. Baberschke, *J. Magn. Magn. Mater.* **2000**, *222*, 163.
[48] Y. Matsumoto, M. Koinuma, S. Ida, S. Hayami, T. Taniguchi, K. Hatakeyama, H. Tateishi, Y. Watanabe, S. Amano, *J. Phys. Chem. C* **2011**, *115*, 19280.
[49] A. F. Gross, M. R. Diehl, K. C. Beverly, E. K. Richman, S. H. Tolbert, *J. Phys. Chem. B* **2003**, *107*, 5475.
[50] W. S. Hummers, R. E. Offeman, *J. Am. Chem. Soc.* **1958**, *80*, 1339.